Loaded Behavior of Gears Made of Fiber-Reinforced PA6

J. Cathelin, J.-P. de Vaujany, M. Guingand and L. Chazeau

This paper presents an original method for computing the loaded mechanical behavior of fiber-reinforced polymer gears. Although thermoplastic gears are unsuitable for application transmitting high torque, adding fibers can significantly increase their performance. The particular case of polyamide 6+30% glass fibers is studied in this paper.

Introduction

The LaMCoS laboratory (*Ed.'s Note: a joint research laboratory of the French National Institute of Applied Sciences and National Centre for Scientific Research*) has developed several numerical models to predict essential results such as load sharing, tooth root stress, contact pressure and transmission error for different types of gears made with elastic or visco-elastic materials. These include, for example, cylindrical gears (Ref. 1); face gears (Ref. 2); spiral bevel gears (Ref. 3); pinion racks (Ref. 4); and worm gears (Ref. 5). To determine load sharing, LaMCoS uses an approach that focuses on solving the displacement/compatibility equation. The influence coefficients method (Ref. 6) is also used and the contact and volume effects are separated; this method is much less time consuming.

Polymer gears are being used in increasing applications due to their low material and manufacturing costs. They also present some advantages unmatched by steel gears in that they can be used without lubricant, their meshing is quieter, and they are lighter. However, they have poor heat resistance and are limited to rotation transmission. In order to improve polymer gear performance, glass fiber is being increasingly used where their lower cost and higher

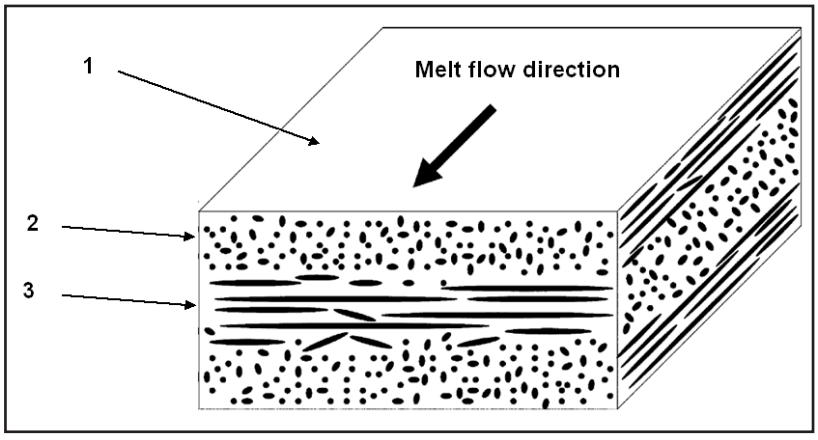

Figure 1 Fiber orientation in a unidirectional flow (Ref. 10).

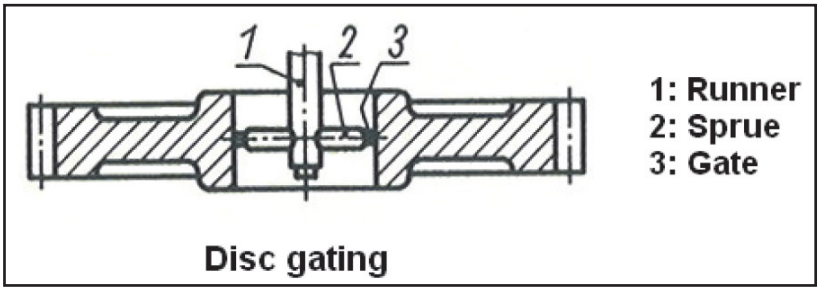

Figure 2 Gating location (Ref. 11).

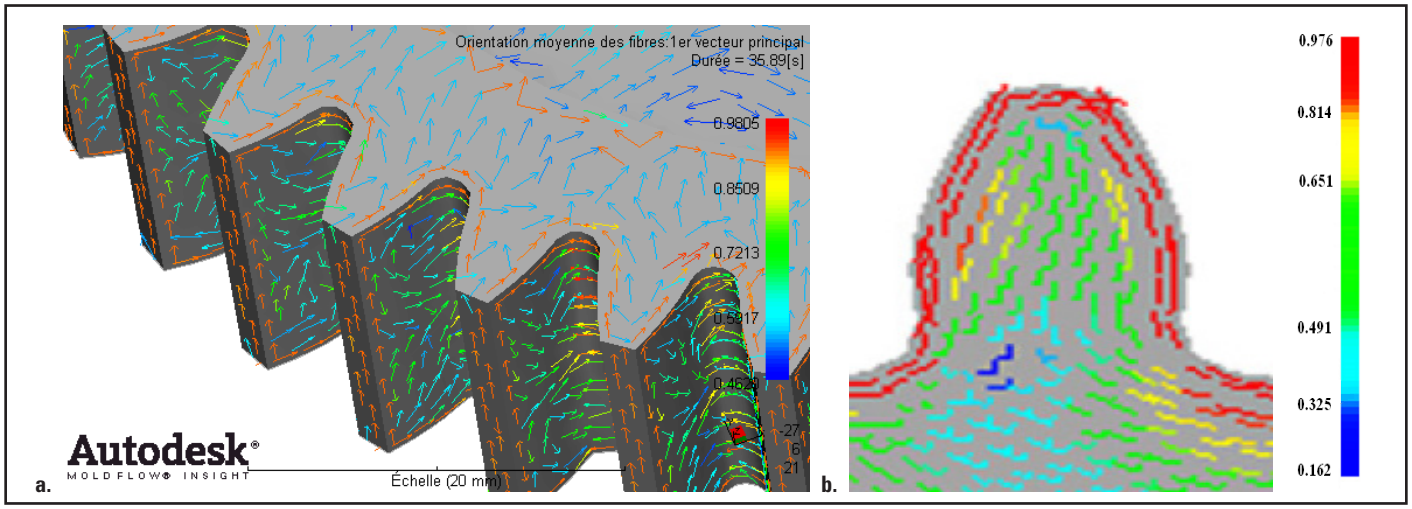

Figure 3 Shell fiber orientation (a); and core orientation fiber in teeth (b).

This paper was first presented at the 2013 VDI International Conference on Gears, Technical University of Munich, Garching, Germany, and is reprinted here with VDI permission

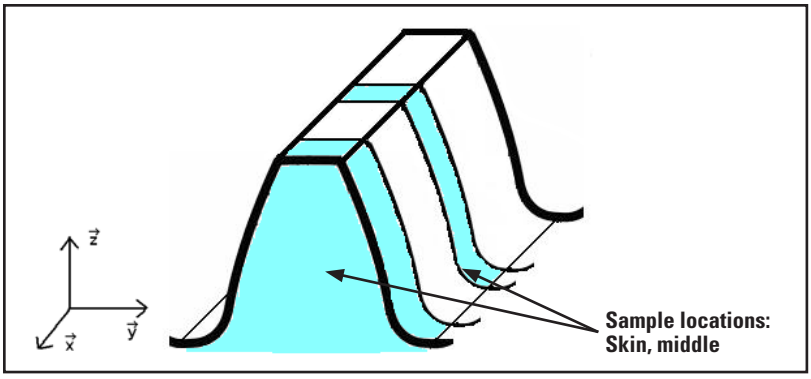

Figure 4 Sample location on teeth.

strength, when compared to unreinforced polyamide, offer a potential increase in gear performance (Ref. 7).

More recently, Hiltcher et al (Ref. 5) developed a quasi-static load-sharing model in the case of a polyamide 66 wheel-and-steel worm. Based on this model Letzelter et al (Ref. 8) developed a quasi-static, load-sharing model in the case of polyamide 66-machined spur gears, taking into account visco-elastic properties and temperature dependence. But unlike the work by Letzelter (Ref. 8) and Hiltcher (Ref. 5), in this paper the gears were molded and the material is anisotropic due to the addition of the glass fibers. Thus this study is limited to the linear domain of the material and it is assumed that the tooth is relaxed for each rotation.

Numerical examples are presented to show the load-sharing and transmission error, depending on the fiber orientation model as well as the elastic and viscous displacement contribution.

Fiber-Orientation in a Molded Gear

Generally concerned fiber orientation. The fiber orientation and distribution in an injection-molded component is dependent on component geometry, molding conditions (gating, temperature, pressure and holding time), matrix material, polymer viscosity and fiber type (aspect ratio, density and volume fraction) (Ref. 9).

The shear forces are dominant in the shell structure orientation. In the shell area, high shear forces tend to align fibers along the melt flow direction. However, in the middle of the core region, shear forces are annulled and so the fiber orientation is situated in the transverse flow direction. Figure 1 shows the schematic of reinforced, glass fiber orientation in a unidirectional flow.

Molding conditions. In this study a disc gating solution (Fig. 2) is used that has the best filling and fiber orientation regularity (Ref. 11).

The cavity geometry, molding conditions and cooling conditions are obtained thanks to commercial molding process simulation software.

Fiber orientation. Fiber orientation simulations were conducted and compared to tomographical, experimental observations. The polymer used is the same in the simulation and for tomographical observations. Figure 3 shows fiber orientation on shell (a) and fiber orientation in the core zone (b). The anisotropy parameter corresponds to the first tensor order and varies between 0 and 1. Number 1 indicates the perfect alignment of the fibers parallel to the reference direction, and 0 is the case of perfect perpendicular alignment with the reference direction.

A quantitative examination has been carried out using tomographic microscopy machines. Sample locations are described in Figure 4; observations are presented in Figure 5.

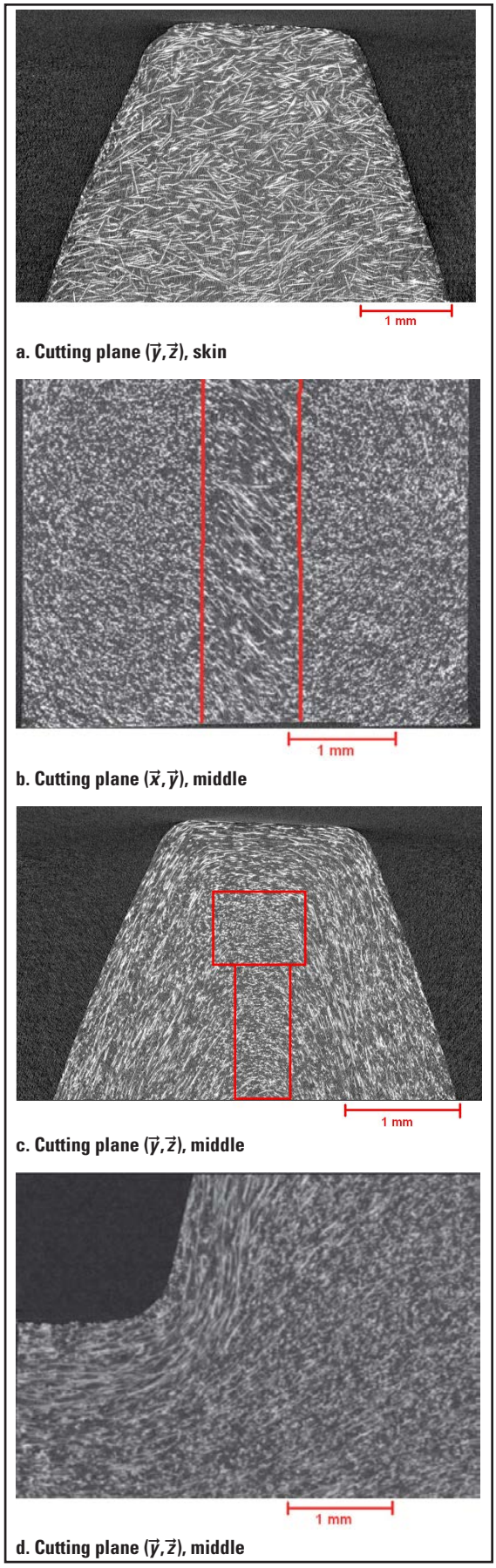

a. Cutting plane ($\vec{y},\vec{z}$), skin

b. Cutting plane ($\vec{x},\vec{y}$), middle

c. Cutting plane ($\vec{y},\vec{z}$), middle

d. Cutting plane ($\vec{y},\vec{z}$), middle

Figure 5 Disc gating gear: $Z=41$; $m=3$.

A comparison between quantitative, simulated fiber orientation prediction and the qualitative, tomography observations reveals similar trends — i.e., three main fiber organization areas are defined: one on the tooth flank, one in the core zone of the teeth, and the last in the root area (Fig. 6).

Mechanical Modeling of Polyamide 6+30% GF

The mechanical behavior of polyamide is viscoelastic in that it depends on loading duration or, in other words, on the history of displacement and temperature. Humidity is another factor to be taken into account in the specific case of polyamide 6.

In order to simulate the wide relaxation time spectrum of polyamide, a generalized Kelvin model is used (Ref. 12) (Fig. 7).

In order to compute the load-sharing, knowledge of the temporal displacement of polyamide 6 material is necessary. The total strain of the generalized Kelvin model is computed in Equation 2. This requires the use of an incremental scheme based on differential Equation 1; the relationship of Equation 1 can be written in each block of the model:

$$\sigma(t) = \frac{1}{\Delta J_i}\varepsilon^i(t) + \frac{\tau_i}{\Delta J_i}\varepsilon^i(t) \quad (1)$$

τ_i is the retardation time; i the index of the block in the generalized Kelvin model; and n is the number of blocks in the model.

$$\varepsilon(t) = \sigma(t)\sum_{i=0}^{n}\Delta J_i\left(\frac{\Delta t}{\Delta t+\tau_i}\right)\sum_{i=0}^{n}\varepsilon^i(t-dt)\left(\frac{\tau_i}{\Delta t+\tau_i}\right) \quad (2)$$

With the relationship of Equation 2, the viscoelastic displacement $u(t)$ is then deduced (Eq. 3):

$$u(t) = l.\sigma(t)\sum_{i=0}^{n}\Delta J_i\left(\frac{dt}{dt+\tau_i}\right) + \sum_{i=0}^{n}u^i(t-dt)\left(\frac{\tau_i}{dt+\tau_i}\right) \quad (3)$$

l is the length of the polyamide 6 specimen (small displacement assumption).

The relationship in Equation 3 is thus used to solve the load-sharing problem. But before doing so, it is necessary to determine the viscoelastic properties ΔJ_i and τ_i.

Results and Viscoelasticity Modeling

Using polymer material, the time-temperature superposition principle can be applied. With this principle and the spectrometer tests — also known as DMA (dynamic mechanical analysis) — it is possible to build, at a given reference temperature, the storage compliance curve $J'(i\omega, T_{ref})$ or the loss compliance curve $J''(i\omega, T_{ref})$, over a very wide frequency range. This curve, known as the "master curve," is obtained from the shift of experimental DMA curves obtained at different temperatures.

In order to determine the distribution of the retardation time τ_i, the numerical Master Curves $J'(i\omega, T_{ref})$ is necessary. It is determined by fitting the Master Curve with a phenomenological model. To do so, the biparabolic model (Eq. 4) developed by Decroix et al. is used (Ref. 13).

$$J^*(i\omega, T_{ref}) = \frac{1+\delta(i\omega\tau')^{-x}+(i\omega\tau')^{-x'}}{\frac{1}{J_u}-\frac{1}{J_r}} + \frac{1}{J_r} \quad (4)$$

To obtain the time spectrum, a discretization by pulsation step of the numerical Master Curve of storage compliance $J'_i(i\omega, T_{ref})$ is needed. In this study, 25 elements of Kelvin Voigt in the Kelvin-

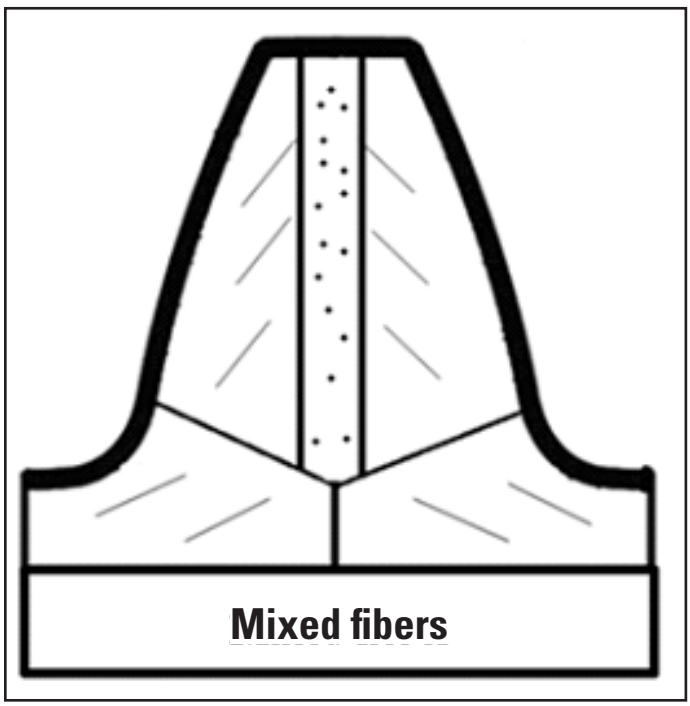

Figure 6 Fiber distribution outline.

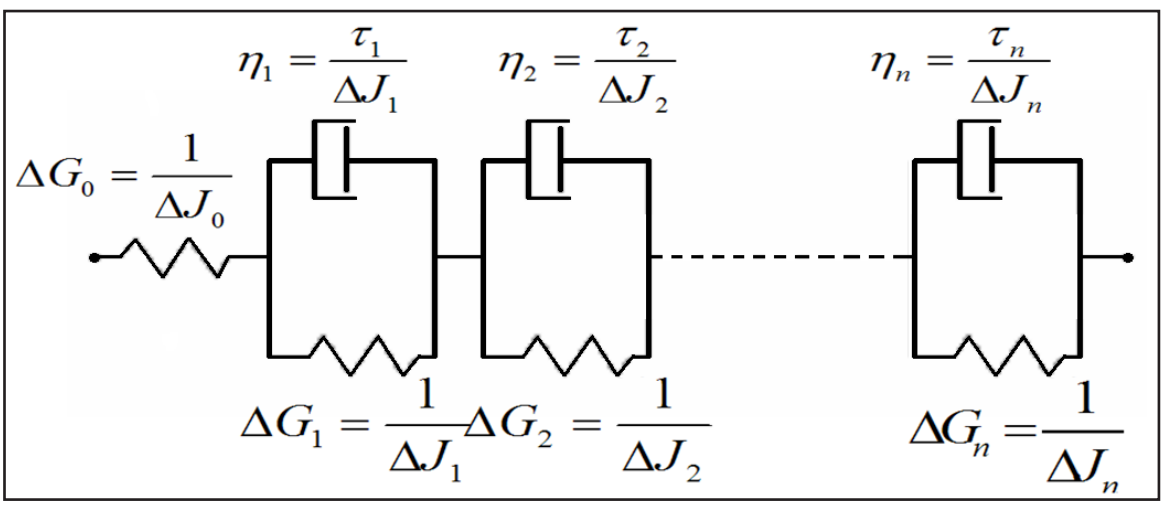

Figure 7 Generalized Kelvin model.

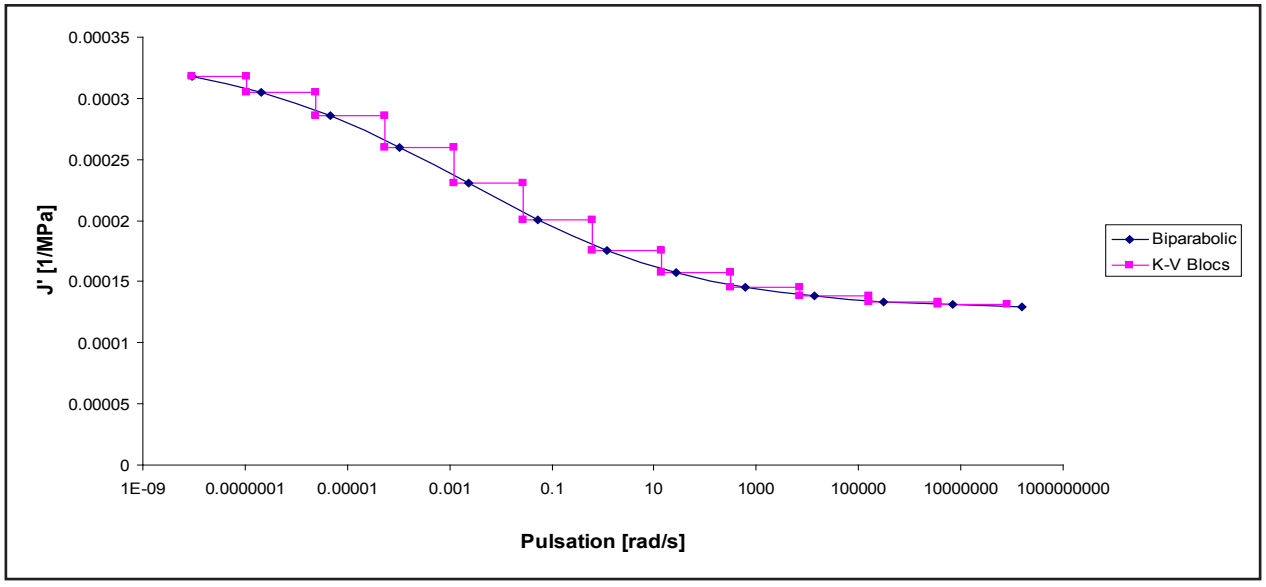

Figure 8 Discretization of the master curve.

generalized model are necessary to take into account a large relaxation time spectrum of the polyamide 6. The distribution of retardation time $\tau_i(T_{ref})$ is deduced from pulsation ω_i at the maximum of $J''_i(i\omega, T_{ref})$; i.e. — in the middle of the frequency segment. The retardation times are deduced with the relationship shown in Equation 5. Figure 8 shows a Master Curve built at the glass transition temperature of 60°C, with fiber parallel to the solicitation direction.

$$\tau_i = \frac{1}{\omega_i} \tag{5}$$

Shift factors $a_{Tref}(T)$ — obtained via the time-temperature superposition principle — enable deducing the retardation time spectrum at temperature T, from the retardation time spectrum obtained at T_{ref} as follows:

$$\tau_i(T) = \tau_i(T_{ref}).a_{T_{ref}}(T) \tag{6}$$

Humidity influences the evolution of viscoelastic properties. Letzelter et al (Ref. 8) assumed that humidity has a similar effect as the temperature on the retardation time spectrum. Within this assumption, a relationship (Eq. 6) can be modified to integrate the relative humidity:

$$\tau_i(T,RH) = \tau_i(T_{ref},Dry).a_{T_{ref},dry}(T).b_{Tref}(RH) \tag{7}$$

The linear viscoelastic properties of polymers can be deduced from spectrometer test DMA.

Load-Sharing Model

The numerical model is based on the procedure developed at LaMCoS. Instantaneous quasi-static studies are computed for steel and polyamide 66 gears (Fig. 9). This procedure is divided into three principal steps. Initially, tooth geometry is obtained with tooth corrections adapted to molded gears; the second step consists of an unloaded kinematics simulation to determine the potential contact zones, while the third step achieves the computation of load sharing between all teeth in contact. This third step integrates the viscoelastic displacement and the loading history in the case of PA6 + 30% GF material. The method yields some results, such as instantaneous pressure distribution, transmission error, load sharing, etc.

For polymer gears it is necessary to know the displacement history of gear and pinion. Consequently, the meshing developed for the polymer gears covers the entire tooth surface. The displacements of pinion and gear are saved for each kinematics position and injected into the next one in order to account for the material relaxation.

The equation of compatibility of displacement. The load-sharing problem consists of solving the equations of displacement compatibility (Eq. 8) while balancing the driving torque (Eq. 9).

$$p(M_k).e(M_k) = p(M_k).(\delta(M_k) + u(M_k) - \alpha) = 0 \tag{8}$$

$$C_{moteur} = \sum_{k=0}^{K} (p_k s_k n_k \wedge M_k) \tag{9}$$

K is the number of nodes of the meshing;
$P(M_k)$ is the contact pressure at point M_k
$e(M_k)$ is the gap between the profiles of the gear and pinion at point M_k after loading
$\delta(M_k)$ is the gap between the profiles of the gear and pinion at point M_k before loading

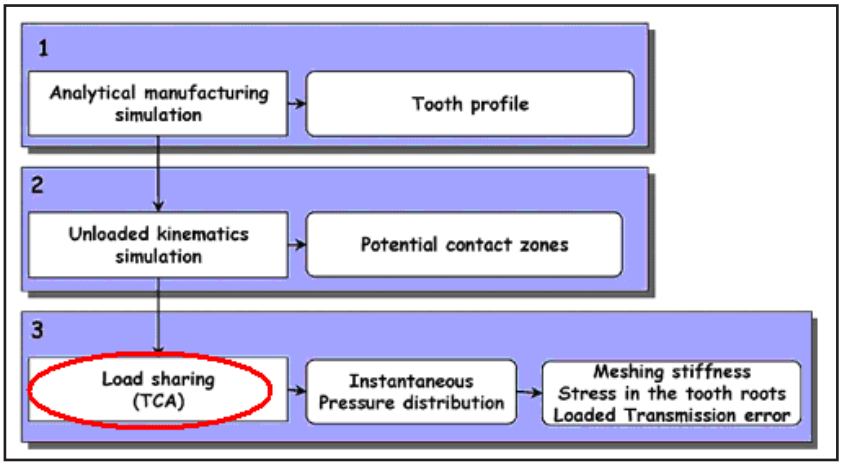

Figure 9 Computing process.

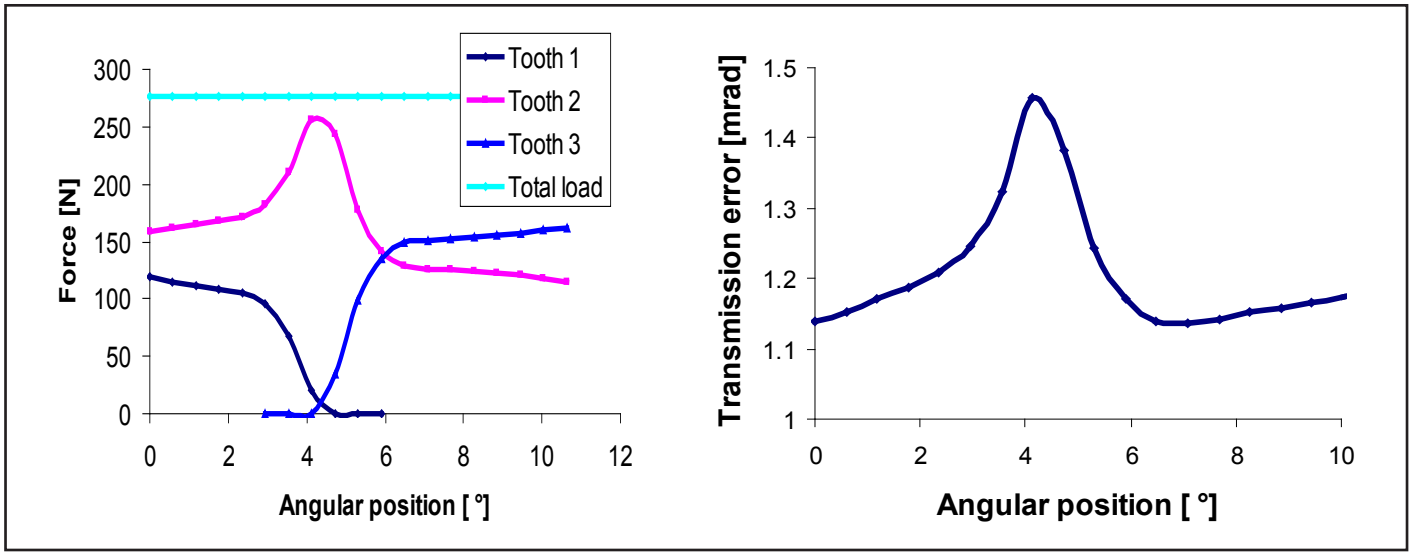

Figure 10 Load-sharing model (a); transmission error at 25°C, 50% of relative humidity, 300 rpm and 15 Nm (b).

$u\,(M_k)$ is the displacement at point M_k and α is the global body adjustment

The influence coefficient. In order to solve the load-sharing problem, it is necessary to compute the displacement u_k, depending on pressure p_k. It is possible to write the relationship (Eq. 10) between the displacement and the pressure with the method of the influence coefficients C_{kj}. There are two types of influence coefficients — the geometrical bulk influence coefficients C_{kj}^V obtained with a standard finite element method, and the contact influence coefficients C_{kj}^S computed with the Boussinesq theory.

(10)

$$u_k = \sum_{j=1}^{K} C_{kj} p_j \text{ with } C_{kj} = C_{kj}^V + C_{kj}^S$$

With the polymer gears the surface geometrical influence coefficients are not linked with the material's compliance; they are defined by the relationship found in Equation 11:

(11)

$$C_{kj}^S + J_{mat}\, C_{kj}^{*S}$$

The geometrical bulk influence coefficient method is obtained in the case of an elastic material. They are computed on gear geometry where the fiber orientation is taken into account in each section (Fig. 6); they are defined by the relationship found in Equation 12:

(12)

$$C_{kj}^V + J_{mat}\, C_{kj}^{*V}$$

The viscoelastic displacement on meshing. In order to determine the nodes displacement in the meshing, the displacement $u_k\,(t)$ is determined (Eq. 12) by the link between the relationships found in Equations 3, 10, 11 and 12.

(13)

$$u_k(t) = \sum_{i=0}^{n} u_k^i(t)$$

(14)

$$u_k^i(t) = \sum_{j=0}^{K} \left[C_{kj}^{*V} p_j(t)\, \Delta J_i^V \left(\frac{\Delta t}{\tau_i + \Delta t} \right) + C_{kj}^{*S} p_j(t)\, \Delta J_i^S \left(\frac{\Delta t}{\tau_i + \Delta t} \right) \right] u_k^i(t - dt) \left(\frac{\tau_i}{\tau_i + \Delta t} \right)$$

ΔJ_i^V represents the bulk storage compliance of polyamide 6 matrix behavior for each block. ΔJ_i^S represents the surface storage compliance of polyamide 6 behavior for each block. Moreover, ΔJ_i^s acknowledges the presence of fibers perpendicular to the solicitation direction.

τ_i remains the same for the surface and bulk material, with the assumption that fiber doesn't affect the viscoelastic behavior of the polyamide 6 matrix. Indeed, τ_i can be adapted to the surface and bulk temperature by the link between the relationship of Equation 7 and the thermal behavior equations proposed by VDI 2736 (Ref. 14).

Numerical Results

Generality. The gear data of the studied gears are shown in the Table 1.

Table 1 Gear data

	Pinion	Gear
Module (mm)	3	3
Pressure angle (°)	20	20
Number of teeth	32	41
Tooth width (mm)	20	20

Figure 10 (a) shows the load-sharing simulated; Figure 10 (b) shows the transmission error simulated for polymer gears during the meshing of one tooth at 25°C and 50% relative humidity, 300 rpm, and 20 Nm. Figure 10 (a) shows a correct shape for the simulated load-sharing. Tooth -1 is unloaded and Tooth 1 is loaded gradually. Tooth 0 — i.e., the central tooth — remains constant. The sum of three forces is equal to a constant force created by the driving torque.

Fiber orientation influence. Three different fiber organization models were used:

- **Case 1**: ***Homogeneous model***:
  Halpin Kardo mixture (Eq. 15) is used to describe the fiber influence (Ref. 15):

  (15)

  $$E_{3D} = 0.184 \times E_{//} + 0.816 \times E_{\perp}$$
- **Case 2: *Unidirectional model***:
  3D stiffness matrix is used for each material section represented in Figure 6.
- **Case 3: *Anisotropic model closed to the tomographical and simulation observations.***

These three models are implemented on standard finite element software in order to obtain the influence coefficients C_{kj}^{V}.

A review of the results reveals that the tooth root stress and contact pressure were minimally impacted by the three models; differences remained under 3%.

Regarding the contact pressures, the material models remain the same at the surface in all three cases. Fibers are always perpendicular to the solicitation direction. This similarity results in equal contact displacements and contact pressure.

Regarding the tooth root stress, this is explained by a low load-sharing change among the different cases.

Table 2 represents the transmission error amplitude in (mrad) where Model 3 is considered the reference.

Differences between the three models did not exceed 8%; the greatest difference between the three models corresponds to the cases where the tooth bending is the most important at 20N-m and 100°C.

Tooth bending displacements. Displacements are observed at the highest contact line. They correspond to the wheel and pinion bending displacement in the case of a tip circle contact of the pinion. Corresponding gear data is found in Table 1; measured displacements take into account the bulk and contact displacements. Also, for both of them the elastic, viscous, and historic origins of displacements are measured. Figure 11 represents the total displacement of pinion and gear at the highest contact point — dependent upon torque and temperature at different rotation speed levels. Total displacements are strongly impacted by temperature and torque, whereas rotation speed has minimal influence.

Bulk and contact displacements. Bulk and contact displacements are distinguished in the displacement equation (Eq. 14) that allows for a separate evaluation of their value. Figure 12 represents the bulk displacements (%) compared to the total displacement at the highest contact line and at different rotation speeds from 10 – 1,000 rpm. It can be noticed that contact displacement plus surface displacement correspond to 100% total displacements.

A look at Figure 12 shows that the bulk displacements are dominant and strongly influenced by the temperature where they represent 85% of the total displacements at 120°C, whereas they represent 65% at 40°C.

Influence of the history of displacements. It is assumed that the tooth is relaxed for one gear rotation. However, the history of displacement due to load just before the tooth arrives in the contact area (2 pitch taken into account) between each quasi-static position is addressed accordingly. An investigation of the influence of history displacement dependent upon temperature, torque and rotation speed has been completed. Displacements are observed at the highest contact line. Results are presented in Figure 13 and the gear data correspond to that found in Table 1.

The history of the displacement is mainly impacted by temperature; at the glass temperature transition and 10 rpm, the history of the displacement represents 18% of total displacement.

Displacements reach their highest value at the glass temperature. It is apparent that

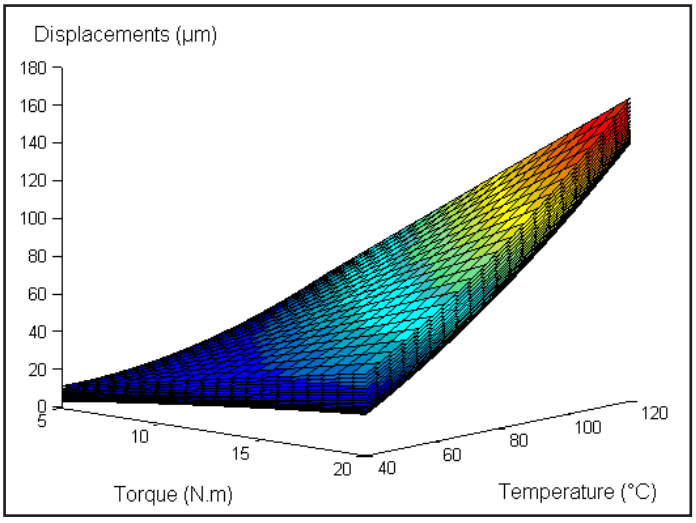

Figure 11 Total tooth displacements at the highest contact point at different rotation speed levels (10–1,000 rpm), Rh = 0%.

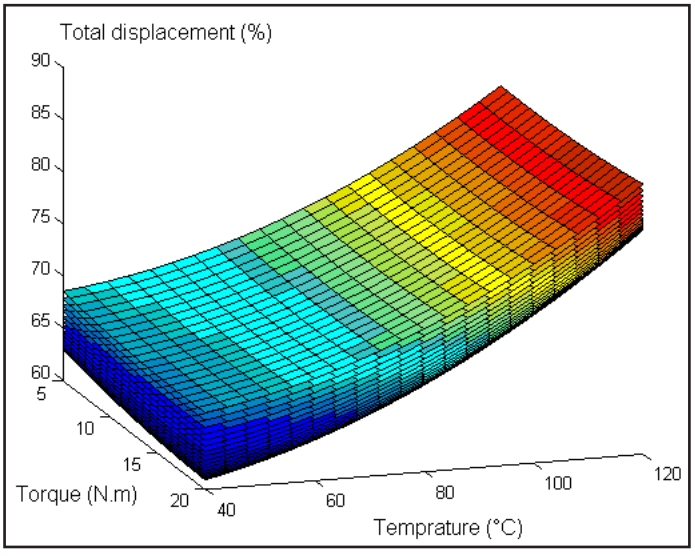

Figure 12 Bulk displacements (%) of the total displacement at the highest contact regarding the bulk displacements at different rotation speed level (10–1,000 rpm), Rh = 0%.

Table 2 Transmission error depending on temperature, torque and model

	T = 0°C		T = 60°C		T = 100°C		
Model 1	0.125	7.4%	0.142	7.2%	0.274	0.7%	C = 5N-m
Model 2	0.132	2.2%	0.150	1.9%	0.272	1.5%	
Model 3	0.135		0.153		0.276		
Model 1	0.285	2.4%	0.286	0.7%	0.233	6.8%	C = 12.5N-m
Model 2	0.288	1.3%	0.280	1.4%	0.221	1.3%	
Model 3	0.292		0.284		0.218		
Model 1	0.304	3.7%	0.278	7.7%	0.206	8.1%	C = 20N-m
Model 2	0.288	1.7%	0.253	1.9%	0.230	2.6%	
Model 3	0.293		0.258		0.224		

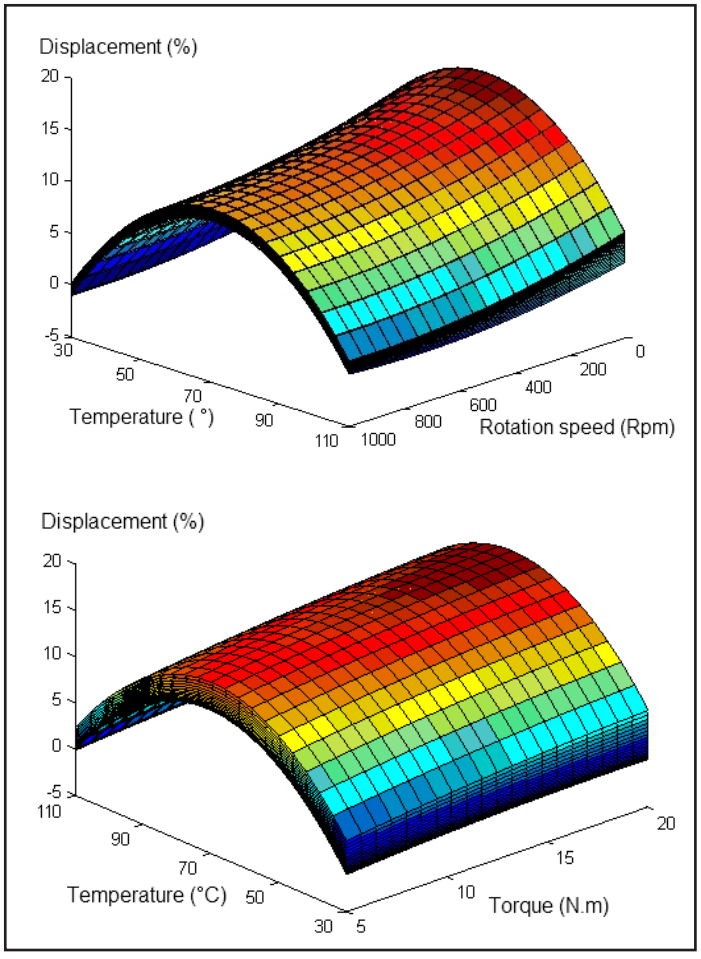

Figure 13 Historic displacements (%) of total displacement (a) depending on temperature and rotation speed at different torque levels (0–20 N-m.); (b) function of temperature and torque at different rotation speed levels (10–1,000 rpm), Rh = 0%.

at low rotation speed (Fig. 13 (a)) the history of displacement impact is more significant, which is attributed to the longer loading time.

Conclusion

This study presents a fast and efficient method to predict the mechanical behavior of polyamide 6 + 30% GF spur gears meshing. The visco-elastic properties are simulated with the generalized Kelvin model. This model takes into account speed, temperature, humidity and fiber orientation. With the viscoelastic displacement and the method-of-influence coefficients calculated over the entire surface of the tooth, it is possible to solve the load-sharing problem.

The computation time is reasonable — i.e., 40 min for 17 quasi-static kinematics positions. Also, this model allows simulation of the fiber amount and orientation influence. Unidirectional models — compared to homogeneous versions and based on a rule of mixture and realistic fiber orientation models — reveal a difference of less than 8% regarding the transmission error amplitude and less than 3% regarding contact pressure and tooth root stresses. The calculated results confirmed that the variation of temperature, humidity and rotation speed can have a considerable influence on the history of displacement, and so they must be taken into account in any model devoted to plastic gears.

References

1. Guingand, M., J.P. De Vaujany and Y. Icard. "Fast, 3D Quasi-static Analysis of Helical Gears Using the Finite Prism Method," *Journal of Mech. Des.*, ASME, 2004, 6 (126), pp. 1082–8.
2. Guingand, M., J.P. De Vaujany and Y. Icard. "Analysis and Optimization of the Loaded Meshing of Face Gears," *Journal of Mech. Des.*, ASME, 2005, 1(127), pp. 135–43.
3. De Vaujany, J. P., M. Guingand, D. Remond and Y. Icard. "Numerical and Experimental Study of the Loaded Transmission Error of a Spiral Bevel Gear," *Journal of Mech. Des.*, ASME, 2007, 2 (129), pp. 129–35.
4. Guingand, M. and J.P. De Vaujany. "Geometry, Kinematics and Load-Sharing of Pinion Rack Gear with Variable Ratio," JSME International Conference on Motion and Power Transmissions, 2009, pp. 13-15.
5. Hiltcher, Y. M. Guingand and J.P. De Vaujany. "Load-Sharing of a Worm Gear with a Plastic Wheel," *Journal of Mech. Des.*, ASME 2007, 1(129), pp. 23–30.
6. Teixeira Alves, J., M. Guingand and J.P. De Vaujany. "Set of Functions for the Calculation of Bending Displacements for Spiral Bevel Gear Teeth," *Mechanism and Machine Theory*, Volume 45, 2010, pp. 349–363.
7. Senthilvelan, S. and R. Gnanamoorthy. "Effect of Rotational Speed on the Performance of a Unreinforced and Glass Fiber-Reinforced Nylon 6 Spur Gear," *Materials and Design*, Vol.28, 2007, pp. 765-772.
8. Letzelter, E., J.P. De Vaujany, L. Chazeau and M. Guingand. "Quasi-static Load-Sharing Model in the Case of Nylon 6/6 Cylindrical Gears," *Materials and Design*, Volume 30, 2009, pp. 4360-4368.
9. Beaumont, J.P., R. Nagel and R. Sherman. *Successful Injection Molding Process — Design and Simulation*, Hanser Publishers, Munich, 2002.
10. Senthilvelan, S. and R. Gnanamoorthy. "Influence of Reinforcement on Composite Gear Metrology," *Mechanism and Machine Theory*, Volume 43, 2008, pp. 1198-1209.
11. Erhard, G. and E. Strickle. Maschinenelemente aus Thermoplastischen Kunststoffen, VDI Verlag, 1976.
12. Ferry, J.D. *Viscoelastic Properties of Polymers*, 3rd Ed., New York, John Wiley, 1980.
13. Decroix, J. Y., A. Piloz, A. Douillard, J.F. May and G. Valet. "Mathematical Model for Viscoelastic Behavior of Poly-a-olefins; Application to Polyolefin Blends and to Hexane-1- Propene Copolymers," *Eur Polym Journal*, 1975, 11, pp. 625–30.
14. VDI 2736 Blatt 2, Thermoplastische Zahnräder, Stirnradgetriebe Tragfähigkeitsberechnung, 2013.
15. Halpin, J.C. and J.L. Kardos. "The Halpin-Tsai Equations: A Review," *Polymer Engineering and Science*, Volume 16, 1976, pp. 344-352.

Julien Cathelin, University of Lyon, INSA Lyon, LaMCoS UMR

Jean-Pierre de Vaujany, University of Lyon, INSA Lyon, LaMCoS UMR

Michele Guingand, University of Lyon, INSA Lyon, LaMCoS UMR

Laurent Chazeau, University of Lyon, INSA Lyon, MATEIS UMR